Herrier J.-L., J. Mees, A. Salman, J. Seys, H. Van Nieuwenhuyse and I. Dobbelaere (Eds). 2005. p. 153-163
Proceedings 'Dunes and Estuaries 2005' – International Conference on Nature Restoration
Practices in European Coastal Habitats, Koksijde, Belgium, 19-23 September 2005
VLIZ Special Publication 19, xiv + 685 pp.

Potentials of airborne hyperspectral remote sensing for vegetation mapping of spatially heterogeneous dynamic dunes, a case study along the Belgian coastline

Luc Bertels[1], Bart Deronde[1], Pieter Kempeneers[1], Sam Provoost[2] and Evy Tortelboom[3]

[1] Remote Sensing and Earth Observation Processes, Flemish Institute for Technological Research
Boeretang 200, B-2400 Mol, Belgium
E-mail: luc.bertels@vito.be

[2] Institute of Nature Conservation
Kliniekstraat 25, 1070 Brussel, Belgium

[3] Afdeling Ondersteunend Centrum GIS-Vlaanderen, Vlaamse Landmaatschappij
Gebroeders Van Eyckstraat 16, 9000 Ghent, Belgium

Abstract

The coastal defence and nature conservation authorities from the Ministry of the Flemish Community need detailed vegetation maps of the Belgian coast for policy planning and evaluation. From an Integrated Coastal Zone Management point of view, the development of efficient tools serving both authorities is desirable. Therefore new methods for objective, detailed and cost-efficient vegetation mapping are under investigation. This paper focuses on the application of airborne hyperspectral imagery. Two classification methods are used. The standard Spectral Angle Mapper, performed after a Minimum Noise Fraction transform, gives an overall accuracy of 59% with 15 vegetation classes. When using the Optimized Spectral Angle Mapper, the overall accuracy can be increased to 67% using the same 15 classes.

Keywords: Hyperspectral; Classification; Spectral Angle Mapper; Optimized Spectral Angle Mapper; Vegetation Mapping.

Introduction

The dynamic dunes along the Belgian coast are an important ecosystem with respect to nature conservation. They are the habitat of a specific and at least regionally rare wildlife (Provoost and Bonte, 2004). Beside their biological value they serve as a natural seawall, protecting the hinterland against floods. The integration of nature conservation and public safety requires balanced decisions and forms a major topic within the Integrated Coastal Zone Management (ICZM) in Belgium. Present day coastal defence supports an integrated approach in which natural processes are guided rather than opposed.

Vegetation maps are an important tool to support this policy. The coastal defence division (AWZ – 'Afdeling Kust') of the Ministry of the Flemish Community applies vegetation stability maps since the 1980s in order to assess management priorities and prevent uncontrolled, large scale blow outs in the fore dunes. Thematically more detailed maps are used for planning and evaluation of nature management, mainly by the nature division (AMINAL, 'Afdeling Natuur'). These maps provide information on syntaxonomically defined vegetation types and can be linked to priority habitats for conservation.
Until present, these vegetation maps are made by manual photo interpretation. A main objective of the HYPERKART project is investigating the suitability of airborne hyperspectral imaging data for efficient, detailed and objective mapping of dune vegetation along the Belgian coast. Imaging spectrometers have developed rapidly over the past decades. They have more channels with better spectral and spatial resolution, individual bands are only a few nanometers wide while the spatial resolution is often less than one meter. Moreover, computer power, data-transfer and storage capacity have increased considerably in recent years. These developments have made it possible to handle and analyse the large data sets acquired by imaging spectrometers.
Within the project, the Belgian coast was imaged by a hyperspectral airborne flight campaign in July 2004, using the AISA Eagle hyperspectral sensor. Vegetation mapping is achieved by comparing image spectra with reference spectra derived from georeferenced ground truth. Therefore an extensive field survey was carried out. In this study two different supervised classification algorithms were tested to produce the vegetation maps. Beside the classical Spectral Angle Mapper (SAM) classification, an innovative classification algorithm was developed, the Optimized SAM (OSAM), which will exhaust the information content of the reference spectra.

Material and methods

The principle of hyperspectral airborne remote sensing

Light emitted by the sun is partially absorbed, partially transmitted and partially reflected by the different materials on the Earth's surface. The nature of the material determines the degree in which different wavelengths are absorbed, reflected or transmitted. The reflected part of the sunlight determines the 'colour' of the material. Because of this, each material has its own spectral identity by which it can be identified. The principle of airborne hyperspectral remote sensing is based on spectroscopy. From an aircraft a location is imaged in different spectral bands in such a manner that for each pixel a quasi continuous (depending on the number of bands) reflectance spectrum is obtained (Fig. 1). High spectral and spatial resolution images acquired with airborne hyperspectral sensors offer the opportunity to map materials and therefore also vegetation in great detail. The reflected radiance measured by the sensor is converted to reflectance values which are defined as the ratio of the intensity of the reflected light to the intensity of the incoming light in function of the wavelength.

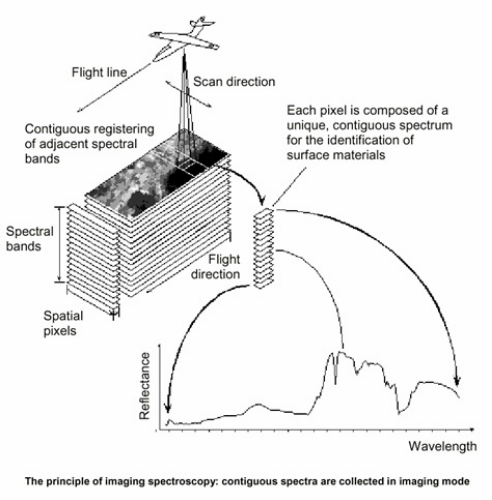

Fig. 1. Principle of airborne imaging spectroscopy.

The typical vegetation spectrum

Sunlight reaching plant leaves is either reflected, absorbed or transmitted. The probability of these processes depends on wavelength, incidence angle and roughness of the leaves as well as on their different optical properties and biochemical composition. The amount of light being absorbed by the leaves as a function of wavelength is selectively determined by the leaf pigments. The visible part of the vegetation reflectance spectrum is characterized by low reflectance values due to very strong absorption of the leaf pigments (Table I).

Table I. Leaf pigments and their absorption maxima

Type of pigment	Characteristic absorption maximum (nm)
Chlorophyll a	420, 490, 660
Chlorophyll b	435, 643
β-Carotene	425, 450, 480
α-Carotene	420, 440, 470
Xanthophylls	425, 450, 475

Absorption is strong in the violet – blue and red part of the spectrum. The green part of the solar spectrum is less absorbed causing plants to exhibit a green colour. Because the energy content of the 'invisible' shortwave infrared part of the solar spectrum is insufficient to trigger photochemical reactions, this part of the energy spectrum is not absorbed by chlorophyll and other leaf pigments. This results in a strong increased reflectance of the near infrared which appears around 690nm and which is typical for vegetation. This is the so-called red-edge. The absorption of the near infrared part of the spectrum is due to the leaf cell internal structure. Fig. 2 shows two arbitrary vegetation

spectra, selected from the hyperspectral image, with an indication of the different spectral features.

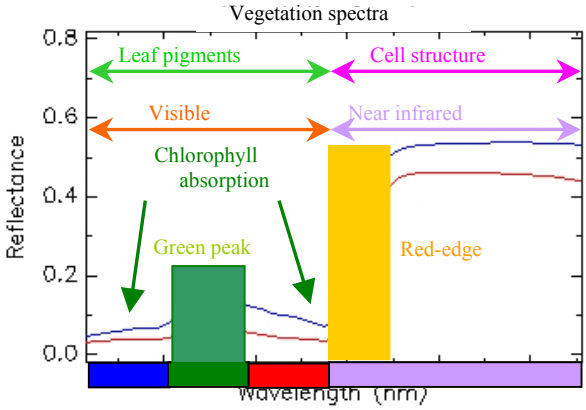

Fig. 2. Typical spectral response characteristic of green plants.

Because different plant species have different leaf pigments, internal cell structure and moisture content, they reflect light in a different way. The relative and often subtle differences between the reflectance in the visible (VIS) and near infrared (NIR) part of the spectrum is used to distinguish between the different vegetation types. Main reflectance features are position and slope of the red-edge, the amount of absorption due to the different leaf pigments in the blue and red part of the spectrum and the amount of reflection at the green peak and at the NIR plateau.

Experimental test site

This study was conducted for a test site called *'De Westhoek'*, in the most western part of the Belgian coast (*De Panne)*. The dune area is about 340ha large and is one of the last unfragmented dune areas along the Belgian coast. *'De Westhoek'* contains most of the (semi-)natural vegetation types that can be found in the Belgian dunes, which suits the requirements of an ideal test area. Floristically, the area is important because of its species richness: almost 400 species of vascular plants have been found in the area, which forms 1/3 of the Flemish flora, and 20% of the species are classified as rare to extremely rare. A quarter of the Flemish Red-List species is present in the *area*. 'De Westhoek' also owes its conservation status to the particular faunal and fungal diversity (Hoys *et al.* 1996).

Ecological consideration

Integrated Coastal Zone Management requires an ecosystem approach of coastal defence. Rather than merely considering dune stability as a state, vegetation should be situated within its ecological functioning. Fig. 3 represents a scheme of the fore dune ecosystem including the most important vegetation patterns and processes. Vegetation mapping should focus on these vegetation characteristics in order to give a

comprehensive image of the ecosystem's functional aspects. Detailed elevation models are very useful ancillary data completing the picture.
Primary dune formation takes place along accreting coasts, where sand is available for embryonic dune formation. Under continuous sand supply these dunes develop towards marram dunes (*Ammophila arenaria*). Decrease of aeolian dynamics will lead to dune fixation with successive development of moss dunes and dune grasslands. Without management of other external 'stress factors', further vegetation succession towards scrub will take place. Vegetation regression caused by internal phenomena such as plant pathogens can change vegetation structure but will not lead to soil degradation. External factors such as trampling or natural blow outs however can lead to soil destruction and initiate secondary vegetation patterns.

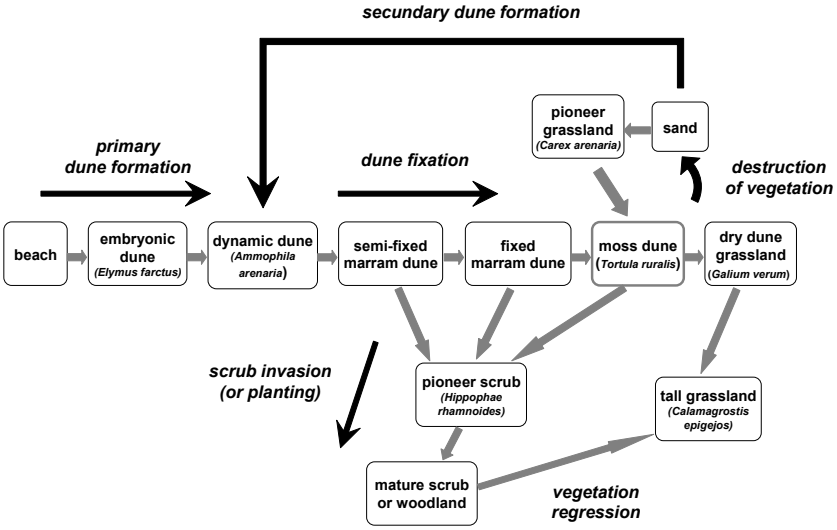

Fig. 3. Scheme of succession relations between coastal dune vegetation types within a landscape ecological framework.

Data acquisition

The AISA Eagle sensor, developed by SPECIM, Spectral Imaging Ltd. Finland, is a complete pushbroom system that consists of a compact hyperspectral sensor head and a miniature 3-axial GPS/INS sensor for monitoring the aircraft position and attitude. Table II gives an overview of the AISA Eagle characteristics.

Band settings and bandwidth are fully programmable and depend on the operation mode. In this study, 32 bands were collected with a ground resolution of 1m x 1m. The selected bands in the green and red region of the solar spectrum and the first part of the NIR-region (between 500nm and 760nm) have a bandwidth (Full Width at Half Max, FWHM) of 2.2nm. This very fine spectral sampling allows to measure the typical vegetation absorption features very accurately. Because the irradiance in the blue region, between 410nm and 500nm, is much lower than in the green, red and NIR part of the

spectrum, the signal to noise ratio in this part is also much lower. By choosing a broader bandwidth in the blue region (FWHM = 25nm), the reflected light is integrated over several channels and the signal to noise ratio is increased. In the NIR region of the vegetation spectrum, the information content is much lower than in the visible part of the spectrum and therefore again a broader bandwidth was chosen (FWHM = 28nm).

Table II. AISA Eagle characteristics

Field of view (FOV)	39.7 DEG
Instantaneous field of view (IFOV)	0.039 DEG
Spatial resolution	0.5 - 10 m
Spectral range	400 - 970 nm
Spectral channels	max. 244
Spectral sampling interval	2.3 nm
Spectral resolution (FWHM)	2.9 nm
Dynamic range	12 bits (4096)

Classification methods

Vegetation classification starting from hyperspectral images can be regarded as a technique for material identification and mapping. The unknown pixels are identified as one of several vegetation types whose reference spectra are derived from the hyperspectral imagery by means of *Regions Of Interest* (ROIs). Ideally, the reflectance spectra of a vegetation type should not vary, but in reality, it does, due to a number of factors, i.e. phenological stage, weather conditions, soil conditions, shadows, *Bidirectional Reflectance Distribution Function* (BRDF) effects, etc.
One of the most frequently applied strategies for material mapping is the use of similarity measures. This study will make use of a deterministic similarity measure to compare an unknown pixel spectrum with a library of reference spectra. *Spectral Angle Mapper* (SAM), is a common distance metric, which compares an unknown pixel spectrum **t** to the reference spectra $\mathbf{r}_i$, $i = 1, ..,K$, for each of K references and assigns **t** to the material having the smallest distance:

$$Class(t) = \arg\min_{1 \le i \le K} d(t, r_i) \quad (1)$$

Collecting ground truth data

During an extensive field campaign, several hundreds of vegetation plots were relevéed and their geographic locations were measured by using a dGPS. Some of the geographic locations were measured as polygons. Because these data were available in 'shape'-format (SHP), it could be easily imported into commercially available image processing software. For homogeneous regions with a minimum diameter of 5m, a point measurement of the central location was performed using the dGPS. The point measurements were used to define ROIs of size 3 by 3 pixels around the central

measured location. Finally, the ROIs were used to extract the pixel spectra which are used as references in the classification algorithm.

Spectral Angle Mapper

The reflectance spectra of individual pixels can be described as vectors in an n-dimensional space, where n is the number of spectral bands. Each vector has a certain length and direction. The length of the vector represents brightness of the pixel while the direction represents the spectral feature of the pixel. Variation in illumination mainly effects changes in length of the vector, while spectral variability between different spectra affects the angle between their corresponding vectors, (Kruse et al., 1993). Fig. 4 shows two three-dimensional spectra, r and t, and indicates the Spectral Angle θ between them. This spectral angle can have values between 0 and π/2 and is calculated as:

$$\theta = \cos^{-1}\left(\frac{\sum_{i=1}^{n} t_i r_i}{\sqrt{\sum_{i=1}^{n} t_i^{\,2} \sum_{i=1}^{n} r_i^{\,2}}}\right) \qquad (2)$$

Where n = the number of spectral bands, t = the reflectance of the actual spectrum and r = the reflectance of the reference spectrum. The more similar the two spectra are, the smaller the spectral angle between them.

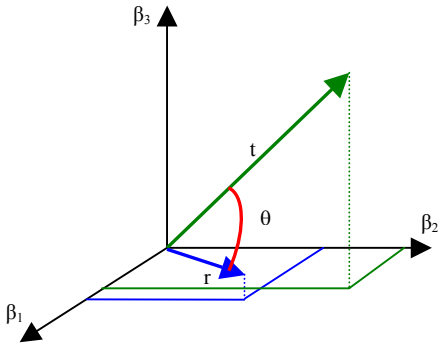

Fig. 4. Visualization of the Spectral Angle θ, between two spectra, t = target spectrum, r = reference spectrum, using three bands β_1, β_2, β_3.

Classification is done by calculating the spectral angles between the reflectance spectrum of the target pixel and the reference spectra. Each pixel will be assigned to the class according to the lowest spectral angle value.

Minimum Noise Fraction

The high spectral and high spatial resolution intrinsic to Imaging Spectroscopy, has an important drawback: imaging spectrometers deliver huge quantities of data. Much of the spectral data in the dataset are redundant. The selection of a small number of relevant spectral bands without loss of essential information for a given application is therefore a critical issue in any Imaging Spectroscopy application. The *Minimum Noise Fraction* (MNF) transform segregates the spectral bands that are dominated by noise from the bands that contain important information, contributing to the overall variance in the dataset. MNF reduces the dimensionality of the dataset and retains the small number of noise-free components. In this way the computational requirements for subsequent processing is reduced (Boardman and Kruse, 1994).
The MNF transform as given in Green *et al.* (1988) is essentially a two-step principle components analysis. The first step calculates a noise covariance matrix and decorrelates and rescales the noise in the data. The second step is a standard principle components transform where the transformed spectral bands are ranked by decreasing explained variance.
The output of the MNF transform is an image cube of n MNF bands. The low-order components have the highest information content, while most of the noise is concentrated in the high ordered bands. The inherent dimensionality can be evaluated by visual examination of the associated images. In the higher order bands surface features are no longer visible and the image is dominated by noise. An other approach to evaluate the cutoff region between signal and noise is to examine the plot of the eigenvalues. Eigenvalues for MNF bands that contain information will be an order of magnitude larger than those containing noise only. The noise-dominated bands have near-unity eigenvalues. Generally most information is concentrated in the lower order MNF bands, but rare spectra may be found in the noisier MNF bands.

Optimized Spectral Angle Mapper

The standard SAM algorithm uses the average spectrum per ROI. This implies that the intra-class variability is not retained. To preserve the intra-class variability an *Optimized Spectral Angle Mapper* algorithm (OSAM) was developed, consisting of two parts.
Firstly, for each class an *Optimal Spectral Library* (OSL) is generated. This library can be considered as 'optimal' since it contains the spectra that classifies as many pixels as possible in the class under consideration, without mis-classifying pixels which do not belong to that class. This is possible thanks to the calculation of the minimum Spectral Angle between a certain spectrum in a class and all pixel spectra which do not belong to the same class as this reference spectrum. In the second step, all pixel spectra are classified using the reference spectra stored in the OSL, i.e. each pixel will be assigned to the class for which the angle between a reference spectrum of that class and that particular pixel spectrum is smallest.

Results and conclusions

All classification experiments were performed with the commercial software package ENVI© Version 4.0. Classification was performed using ground truth data of 15 different

vegetation types. For each vegetation type a number of ROIs were used, ranging from three ROIs for wood small-reed (*Calamagrostis epigejos*) to 23 ROIs for creeping willow (*Salix repens*). After the MNF transformation the standard SAM classification was performed, using the first six MNF-bands. To clean-up the initial classification result, a standard majority 3x3 filter was applied. This filter uses a 3x3 pixels kernel and replaces the center pixel in the kernel with the class value that the majority of the pixels in the kernel has. The obtained overall accuracy reached 59% and was calculated by a confusion matrix using all ground truth ROIs. However, this accuracy is overestimated since training pixels and validation pixels are identical. All accuracies mentioned in this paper are weighted, *i.e.* they take into account the number of pixels per class.
Next, the Optimized SAM classification was applied. Fig. 5 shows the result of the OSAM classification after post-classification clean-up by a majority 3x3 filter.

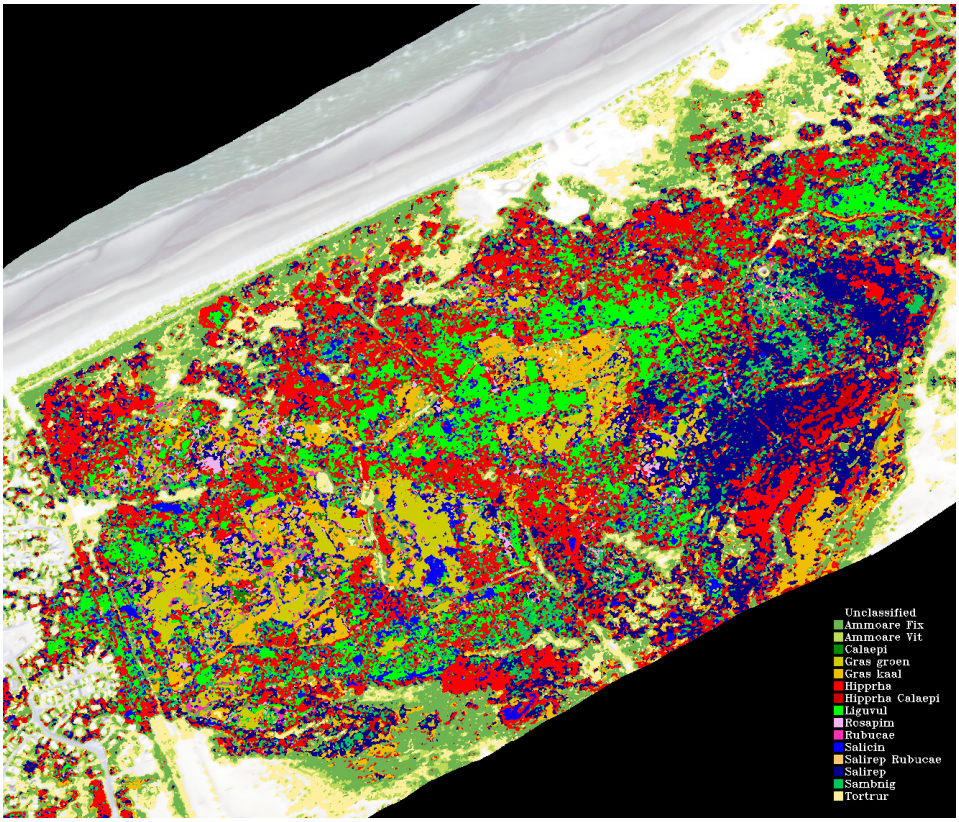

Fig. 5. Classification result obtained by the Optimized Spectral Angle Mapper (OSAM).

75% of the pixels of each class were randomly selected for training while the remaining 25% pixels were used for accuracy calculation. To obtain a statistical significant result, the overall accuracy was calculated as the mean of the accuracies calculated over 20 runs. For OSAM an overall weighted accuracy of 67% was obtained. Compared to the

accuracy obtained with the standard SAM, the accuracy obtained by OSAM can be considered as more valuable because training and validation spectra were separated.

To further increase the accuracy several measures can be taken. Firstly, the hyperspectral images used in this study have a geometric inaccuracy of 1 to 5 pixels. Because wrongly selected ground truth pixels result in bad classification performance, the different ROIs need to be manually repositioned to make sure they select the correct ground truth pixels. Secondly, several vegetation types residing in similar environments, *e.g.* different grassland types, different dune slack types and different pioneer vegetation types, have similar reflectance spectra and therefore are difficult to separate. By lumping these vegetation types the overall classification accuracy can be increased. Thirdly, different users need different vegetation maps. One user might be interested in the distribution of the broader vegetation classes, while the other user might be interested in the very detail of vegetation type distribution. It is obvious that the level of detail will influence the level of classification accuracy, i.e. vegetation maps indicating the broader classes have high accuracy values, while detailed vegetation maps will have lower accuracy values.

Nevertheless, the results obtained by SAM classification methods, especially the OSAM method, yield promising results. They illustrate the potential of using hyperspectral imagery for the generation of detailed vegetation maps, distinguishing a large number of vegetation types.

Acknowledgement

This research is financed by the Belgian Science Policy and by the Flemish Government, Coastal Division. The authors gratefully thank Dr. Carine Petit, Dr. Joost Vandenabeele, ir. Peter De Wolf and ir. Toon Verwaest for their support.

References

Boardman J.W. and F.A. Kruse. 1994. Automated spectral analysis; a geological example using AVIRIS data, north Grapevine Mountains, Nevada. In: Proceedings, ERIM Tenth Thematic Conference on Geologic Remote Sensing, Environmental Research Institute of Michigan, Ann Arbor, I-407 - I-418.

Dennison P.E. and D.A. Roberts. 2003. The effects of vegetation phenology on endmemeber selection and species mapping in southern California chaparral. Remote Sensing of Environment 87:295-309.

Green A.A., M. Berman, P. Switzer and M.D. Craig. 1988. A transformation for ordering multispectral data in terms of image quality with implications for noise removal: IEEE Transactions on Geoscience and Remote Sensing 26(1):65-74.

Hoys M., M. Leten and M. Hoffmann. 1996. Ontwerpbeheersplan voor het staatsnatuurreservaat De Westhoek te De Panne (West-Vlaanderen). Universiteit Gent in opdracht van AMINAL, afdeling Natuur. 267p.

Kruse F., A. Lefkoff, J. Boardman, K. Heidebrecht, A. Shapiro, P. Barloon and A. Goetz. 1993. The spectral image processing system (SIPS) - interactive visualization and analysis of imaging spectrometer data. Remote Sensing of Environment 44:145-163.

Provoost S. and D. Bonte [red.]. 2004. Levende duinen: een overzicht van de biodiversiteit aan de Vlaamse kust. Mededelingen van het Instituut voor Natuurbehoud 22, Brussel. 420p.

Schmidt K.S. and A.K. Skidmore. 2003. Spectral discrimination of vegetation types in a coastal wetland. Remote Sensing of Environment 85:92-108.

Van Der Meer F. and S.M. De Jong. 2001. Imaging Spectrometry. Basic Principles and Prospective Applications. Kluwer Academic Publishers, Dordrecht/Boston/London, 403p.

Van Til M., R. De Lange and A.M. Bijlmer. 2003. Hyperspectrale beeldverwerking voor de kartering van duinvegetatie. Gemeentewaterleidingen Amsterdam.